**This paper is available on line at http://www.mcponline.org**

# Proteomic Analysis of Virus-Host Interactions in an Infectious Context Using Recombinant Viruses*[S]

**Anastassia V. Komarova‡, Chantal Combredet‡, Laurène Meyniel-Schicklin§¶‖, Manuel Chapelle**, Grégory Caignard‡, Jean-Michel Camadro**, Vincent Lotteau§¶‖, Pierre-Olivier Vidalain‡‡‡, and Frédéric Tangy‡‡‡**

**RNA viruses exhibit small-sized genomes encoding few proteins, but still establish complex networks of interactions with host cell components to achieve replication and spreading. Ideally, these virus-host protein interactions should be mapped directly in infected cell culture, but such a high standard is often difficult to reach when using conventional approaches. We thus developed a new strategy based on recombinant viruses expressing tagged viral proteins to capture both direct and indirect physical binding partners during infection. As a proof of concept, we engineered a recombinant measles virus (MV) expressing one of its virulence factors, the MV-V protein, with a One-STrEP amino-terminal tag. This allowed virus-host protein complex analysis directly from infected cells by combining modified tandem affinity chromatography and mass spectrometry analysis. Using this approach, we established a prosperous list of 245 cellular proteins interacting either directly or indirectly with MV-V, and including four of the nine already known partners of this viral factor. These interactions were highly specific of MV-V because they were not recovered when the nucleoprotein MV-N, instead of MV-V, was tagged. Besides key components of the antiviral response, cellular proteins from mitochondria, ribosomes, endoplasmic reticulum, protein phosphatase 2A, and histone deacetylase complex were identified for the first time as prominent targets of MV-V and the critical role of the later protein family in MV replication was addressed. Most interestingly, MV-V showed some preferential attachment to essential proteins in the human interactome network, as assessed by centrality and interconnectivity measures. Furthermore, the list of MV-V interactors also showed a massive enrichment for well-known targets of other viruses. Altogether, this clearly supports our approach based on reverse genetics of viruses combined with high-throughput proteomics to probe the interaction network that viruses establish in infected cells.** ***Molecular & Cellular Proteomics 10: 10.1074/mcp.M110.007443, 1–17, 2011.***

RNA viruses are responsible for numerous human diseases like flu, AIDS, hepatitis C, dengue, measles, yellow fever, and others that still represent major public health threats. Despite small genomes encoding only few viral proteins, RNA viruses establish a complex network of interactions with host cell components to block cellular defense mechanisms and hijack host cell machinery (for review see (1). Deciphering these interactions is essential to reach a comprehensive understanding of the viral infection process. To obtain this information at a system level, high-throughput technologies like yeast two-hybrid or MS-based protein-complex analysis are currently used. However, these strategies have significant limitations.

In the yeast two-hybrid system, viral proteins are used as baits to screen host cDNA or ORFeome libraries. This technology was used to establish a first draft of hepatitis C virus and influenza virus infection networks, and allowed the identification of several cellular pathways as major targets of these viruses (2, 3). Although highly tractable, the yeast two-hybrid technique can be criticized because an artificial interaction assay is performed in a heterologous system. For MS-based proteomics, single tagged viral proteins or viral protein complexes are expressed in host cells, and then isolated together with interacting cellular factors using one-step or tandem affinity purification protocols. For instance, the ribonucleoprotein and polymerase complexes of influenza A virus have been rebuilt in human cells by transient co-expression of tagged viral proteins, and then purified to identify cellular binding partners (4). Although this approach is somewhat more relevant in its design than the yeast two-hybrid system, it can be argued that virus-host interactions are detected in non-infected cells. Alternatively, virions or virus ribonucleoproteins (RNPs or ribonucleocapsid) can be purified from infected cell cultures or tissues using gel exclusion chromatography or appropriate density gradients, and then analyzed for copuri-

From the ‡Unité de Génomique Virale et Vaccination, Institut Pasteur, CNRS URA 3015, Paris, France; §INSERM U851, Lyon, France; ¶IFR128-BioSciences, Université Lyon 1, France; ‖Université de Lyon, France; **Plateforme de Protéomique Structurale et Fonctionnelle, Institut Jacques Monod, Université Paris-Diderot, CNRS UMR 7592, Paris, France

Received January 17, 2011, and in revised form, August 18, 2011
Published, MCP Papers in Press, September 12, 2011, DOI 10.1074/mcp.M110.007443

fied cellular proteins by MS (5, 6, 7). However, this approach is only applicable to viral proteins that assemble into high molecular weight multiprotein complexes. Thus, innovative strategies are needed to detect virus-host protein interactions in infected cell cultures.

The study of RNA viruses has greatly benefited from the ability to engineer viral genomes and generate modified viruses by reverse genetics (for review see (8–10). Interestingly, this technology may be used to generate recombinant viruses carrying amino acid tags in fusion with one or several of their proteins, provided that the tags do not interfere with viral protein functions. Then, tagged viral proteins can be purified directly from infected cells and copurified cellular interactors identified by MS-based analysis. With such tagged viruses in hand, virus-host protein interactions could be identified all along a virus life cycle, within different cell types and under various culture conditions. As a proof-of-concept, we developed and describe in this report such technology for measles virus (MV).[1]

MV is a negative-strand RNA virus from *Paramyxoviridae* family that encodes six structural proteins and two nonstructural virulence factors, among which MV-V has been extensively studied (11). Although MV-V is not essential to viral replication *in vitro*, this protein is required for MV propagation *in vivo* (12, 13). MV-V is encoded by the P locus, and is composed of an N-terminal PNT region and C-terminal VCT region. MV-V is best known for its ability to block type I interferon (IFN-$\alpha/\beta$) pathway by different mechanisms, thus impairing antiviral immune response in MV-infected cells. Accounting for this activity, MV-V has been shown to interact directly with IFIH1 and LGP2 antiviral RNA helicases, JAK1 and IKK-$\alpha$ kinases, and IRF7, STAT1, STAT2, p53, and p73 transcription factors (14–19). Thus, MV-V interacts with multiple cellular components and moonlights between different functions that are essential to viral inhibition of host cell immunity. Consequently, MV-V represents a prototypical viral virulence factor that exerts multiple regulatory functions, thus suggesting numerous dynamic interactions with human proteome. We used a reverse genetic system developed in our laboratory (20) to produce a recombinant MV strain expressing the MV-V protein with a One-STrEP amino-terminal tag. This allowed MV-V purification directly from infected cells using a modified one-step purification approach. Copurified cellular factors were identified by direct MS-based analysis. Already known MV-V cellular partners were recovered with this system but more importantly, a specific and prosperous list of new virus-host interactions was found. To our knowledge, this is the first report describing a combination of reverse genetic with proteomic analysis to map virus-host interactions directly from virus-infected cells. In the future, the same method could be applied to any virus with a negative-strand RNA genome.

## EXPERIMENTAL PROCEDURES

*Cells, Plasmid Constructions, and Rescue of Recombinant Viruses*—HEK-293T (human embryonic kidney) and Vero cells (African green monkey kidney cells) were maintained in Dulbecco's modified Eagle's medium (DMEM)-Glutamax (Invitrogen) supplemented with 10% heat-inactivated fetal calf serum (Invitrogen, Frederick, MD). Stable helper 293-T7-NP cells were used for viral rescue as previously described (21), and grown in Dulbecco's modified Eagle's medium10% fetal calf serum . pTM-MVSchw plasmid, which contains an infectious MV cDNA corresponding to the antigenome of the Schwarz vaccine strain, has been previously described (20, 21).

A two-step PCR-based strategy was used to produce coding sequences for MV-V, MV-N, and the Red fluorescent protein Cherry (CH) with either N- or C-terminal One-STrEP-tags. First, the One-STrEP-tag coding sequence was amplified by PCR from pEXPR-IBA105 using different primer pairs to add a flexible Tobacco Etch Virus (TEV) protease linker (ENLYFQS) either at the N- or C terminus of this sequence. In parallel, DNA fragments corresponding to MV-V, MV-N, or CH coding sequences were amplified using pTM-MVSchw or pmCherry Clontech, Palo Alto, CA) as a template. PCR products were finally combined, and then amplified in a second PCR reaction to recover expected fusion sequences, *i.e.* MV-V and CH with a N-terminal One-STrEP tag, and MV-N and CH with a C-terminal One-STrEP tag (supplemental Fig. S1). These four amplicons contained unique BsiWI and BssHII sites at their extremities for subsequent cloning in pTM2-MVSchw, but were first cloned in pCR2.1-TOPO plasmid (Invitrogen) and sequenced. These plasmids were designated pTOPO/STrEP-V, pTOPO/STrEP-CH, pTOPO/N-STrEP, and pTOPO/CH-STrEP. Finally, sequences were introduced in the additional transcription unit of pTM2-MVSchw vector after BsiWI/BssHII digestion. The resulting plasmids were designated pTM2-MV/STrEP-V, pTM2-MV/STrEP-CH, pTM2-MV/N-STrEP, and pTM2-MV/CH-STrEP. The coding sequence of firefly luciferase (Luc) from *Photinus pyralis* was introduced in pTM2-MVSchw using the same approach. The DNA fragment encoding for Luc was amplified by PCR using pISRE-Luc (Stratagene) as a template. This DNA fragment contained unique MluI and BssHII restriction sites at its extremities for subsequent cloning in pTM2-MVSchw. The resulting plasmid was designated pTM2-MV/Luc. All MV insertions respect the "rule of six," which stipulates that the number of nucleotides of MV genome must

[1] The abbreviations used are: MV, Measles virus N nucleoprotein; CH Red, fluorescent protein Cherry; CHD4, Chromodomain-helicase-DNA-binding protein 4; GATAD2A, Transcriptional repressor p66-alpha; HDAC, Histone deacetylase complex; IFIH1, Interferon-induced helicase C domain-containing protein 1; IFN, Interferon; IKK-$\alpha$, Inhibitor of nuclear factor kappa-B kinase subunit alpha; IRF7, interferon regulatory factor 7; JAK, Tyrosine-protein kinase; LGP2, Probable ATP-dependent RNA helicase DHX58 Luc Firefly luciferase protein; MBD3, Methyl-CpG-binding domain protein 3; MOI, multiplicity of infection; MTA, Metastasis-associated protein; RBBP7, Histone-binding protein; rMV2/Luc, recombinant MV with Luc inserted in an additional transcription unit between P and M ORFs; rMV2/STrEP-CH, recombinant measles virus with Cherry protein possessing N-terminal STrEP-tag inserted in an additional transcription unit between P and M ORFs; rMV2/CH-STrEP, recombinant measles virus with Cherry protein possessing C-terminal STrEP-tag inserted in an additional transcription unit between P and M ORFs; rMV2/STrEP-V, recombinant measles virus with V protein possessing N-terminal STrEP-tag inserted in an additional transcription unit between P and M ORFs; rMV2/N-STrEP, recombinant measles virus with N protein possessing C-terminal STrEP-tag inserted in an additional transcription unit between P and M ORFs; RNP, ribonucleoprotein; STAT, Signal transducers and activators of transcription protein; TEV, Tobacco Etch Virus; TSA, Trichostatin A.

be a multiple of six (22). Recombinant viruses were rescued, and virus titers and single-step growth curves were determined as previously described (21).

A simple PCR amplification strategy was used to subclone STrEP-V, STrEP-PNT, CH-STrEP coding sequences in a mammalian expression vector. STrEP-V and STrEP-PNT were amplified from pTOPO/STrEP-V, whereas CH-STrEP was amplified from pTOPO/CH-STrEP. All three DNA fragments contained unique EcoRI and SalI restriction sites at their extremities for subsequent cloning in pCI-neo (Promega, Charbonnières, France). The resulting plasmids were designated as pCI-neo/STrEP-V, pCI-neo/STrEP-PNT, and pCI-neo/CH-STrEP.

*Antibodies and Western Blots Assays*—Vero cells were infected in 35-mm dishes with MV recombinant viruses at a multiplicity of infection (MOI) of 1. At 24 h postinfection, cells were lysed in 500 $\mu$l of lysis buffer (20 mM MOPS-KOH pH7.4, 120 mM of KCl, 0.5% Igepal, 2 mM $\beta$-Mercaptoethanol), supplemented with Complete Protease Inhibitor Mixture (Roche). Cell lysates were incubated on ice for 20 min, then clarified by centrifugation at 16,000 $\times$ *g* for 15 min. Protein extracts were resolved by SDS-PAGE gel electrophoresis on 4–12% NuPAGE Bis-Tris gels with MOPS running buffer (Invitrogen) and transferred to cellulose membranes with the IBlot Dry blotting system (Invitrogen). To detect One-STrEP-tag and MV proteins, membranes were blotted with either a mouse anti-N mAb (clone 25; kindly provided by Pr. Chantal Rabourdin-Combe (23), or a rabbit polyclonal anti-V rAb kindly provided by Dr. Kaoru Takeuchi (24), or Streptavidin-HRP (Invitrogen, 19534–050). Peroxidase activity was visualized with an ECL Plus Western blotting Detection System (GE Healthcare, RPN2132). STAT1 and STAT2 proteins were revealed using clone-1 (Ref. G16920) and clone 22 (Ref. S21220), respectively (mouse monoclonal antibodies; BD Biosciences). Secondary anti-mouse HRP-conjugated antibodies were from GE-Healthcare.

*Modified One-STrEP Tag Purification*—HEK-293T ($8 \times 10^7$) cells were either infected with MV recombinant viruses at an MOI of 1 or transfected using jetPRIME (Polyplus transfection) with 40 $\mu$g of pCI-neo/STrEP-V or pCI-neo/STrEP-PNT or pCI-neo/CH-STrEP. Twenty-four hours postinfection or post-transfection, cells were lysed in 4 ml of lysis buffer. Cell lysates were incubated on ice for 20 min, and then clarified by centrifugation at 16,000 $\times$ *g* for 15 min. Protein extracts were incubated for 2 h on a spinning wheel at 4 °C with 300 $\mu$l of StrepTactin Sepharose High Performance (GE Healthcare, 28935599). Beads were then washed twice for 5 min on a spinning wheel with 10 ml of washing buffer (20 mM MOPS-KOH pH7.4, 120 mM of KCl, 2 mM $\beta$-Mercaptoethanol), supplemented with Complete Protease Inhibitor Mixture (Roche). Protein complexes were eluted from StrepTactin beads with 0.04 mg/ml of TEV protease (kindly provided by Dr. Nicolas Wolff, Unité de Résonance Magnétique Nucléaire des Biomolécules, Institut Pasteur) in 2 ml of washing buffer overnight on a spinning wheel at 4 °C. Beads were centrifuged at 1600 $\times$ *g* for 5 min at 4 °C to recover eluted protein complexes. Beads were washed once with 2 ml of washing buffer to recover a maximum of protein complexes. Finally, eluted proteins were precipitated overnight at 4 °C with TCA (12% final concentration). Protein pellets were washed twice with ice-cold acetone, and resuspended in deionized water (Mili-Q). Protein concentration was determined using the Amido Schwarz staining reaction (25).

*SDS-PAGE Analysis of Affinity Purified Protein Complexes*—XT Sample buffer (BioRad, Hemel Hempstead, UK; 161–0791) and XT Reducing Agent (BioRad, 161–0792) were added to 10 $\mu$g of protein. After denaturation for 5 min at 100 °C, protein samples were loaded on a precast 4–12% acrylamide gel (BioRad). Gels were stained with Proteo Silver Plus Silver Stain Kit (Sigma, Prot-SIL2).

*Identification of Virus-Host Protein Partners by Mass Spectrometry*—Equal protein concentrations from 0.1 $\mu$g to 1 $\mu$g were used in each nano-LC-MS/MS experiment. Proteins were digested overnight at 37 °C with 20 $\mu$l of a trypsin solution prepared as follow: high-performance liquid chromatography (HPLC) water, 10 ng/$\mu$l trypsin sequencing grade (Roche), 10% HPLC grade acetonitrile, 25 mM ammonium carbonate (Sigma). Resulting peptide extracts were speedvac dried and dissolved in 12 $\mu$l HPLC grade water, 0.1% formic acid. 5 $\mu$l were used for nano-liquid chromatography (LC)-tandem MS (MS/MS) analysis using a nano-chromatography system (Easy nLC, Proxeon) connected online to a LTQ Velos Orbitrap (ThermoFisher) mass spectrometer. A 2 cm long, 5 $\mu$m particle size C18 Easy column (Proxeon) was used for peptide trapping and desalting. A 10 cm long and 3 $\mu$m particle size C18 Easy column (Proxeon) was used for peptides separation. The peptide elution gradient was from 100% buffer A (HPLC grade water, 0.1% formic acid) to 35% buffer B (HPLC grade acetonitrile, 0.1% formic acid) in 60 min using a constant flow of 300 nl/min. MS spectra were acquired on the Orbitrap analyzer at resolution mode $r = 30{,}000$. After each MS spectrum, an automatic selection of 20 most intense precursor ions was activated with 15 s dynamic exclusion delay to acquire MS/MS spectra on the LTQ Velos analyzer, using collision-induced dissociation fragmentation mode at 35% relative resonant activation energy for 40 msec.

Raw data were preprocessed using ProteomeDiscoverer version 1.2 (ThermoFisher). Pre-processing consisted of MS/MS spectrum averaging of spectra from equal precursor molecular weight, with 5 ppm mass tolerance and 90s time window. No thresholding was applied either to MS ions intensities or MS/MS fragment ions intensities.

All spectra were analyzed twice using Mascot version 2.1 (Matrix Science). A first query was performed against a nonredundant database of 20,352 human protein sequences from Swissprot (rel. 57.15) to which corresponding random decoy entries were added. Then, second search was performed against a database made of the 90 MV protein sequences found in the SwissProt database. Each sequence was randomized 11 times and added as decoy to this database, thus resulting in a 1080-entry database suitable for robust and consistent calculation. The sequence of the red fluorescent protein Cherry was also included. Mascot was run in MS/MS Ion search mode with the following parameter settings: no fixed modification, variable modification (oxydation on methionine), precursor mass tolerance 5 ppm, fragment ions mass tolerance 0.4 Da, two missed cleavages, and trypsin as digestion enzyme. Additional filtering was applied after protein and peptide identification for further analysis, using following criteria: for single and multiple peptide hit proteins each Mascot ionscore $\geq$30. Such criteria allowed us to obtain a false-positive rate below 1% for each search, based on numbering of identified decoy entries. For proteins identified on the basis of one unique peptide spectrum see supplemental Fig. S2.

*Protein Interaction Network Analysis*—Interactions between cellular proteins that copurified with MV-V were retrieved from APID ("Agile Protein Interaction DataAnalyzer") using APID2NET plug-in integrated in Cytoscape software, an advanced network analysis tool (26, 27). The obtained interaction network was subsequently analyzed with BINGO2 plug-in to determine statistical enrichments for Gene Ontology (GO) categories (28). Finally, protein nodes were colored using the GOlorize plug-in to emphasize enrichments for specific GO terms (29).

For network topological analyses, and because the APID data set is not accessible as a whole, a human interactome network was reconstructed from IntAct database (30). Intact database is part of the APID data set, and represents 25.7% of interaction data retrieved by APID2NET. Virus-host protein interaction data were from VirHostNet database (31). The R (http://www.r-project.org) statistical environment was used to perform statistical analysis, and the igraph R

package (http://cneurocvs.rmki.kfki.hu/igraph/) was used to compute network metrics. In our topological analyses, the degree *k* of a node in a graph is defined as the number of edges that are incident to this node. It is a local centrality measure that takes into account only direct 1-hop neighbors, *i.e.* direct interacting partners. The betweenness *b* of a node in a graph can be defined by the number of shortest paths going through this node, and is normalized by twice the total number of proteins pairs in the graph. The equation used to compute the betweenness centrality *b* for a node *v* is:

$$b(v) = \frac{1}{n \times (n-1)} \times \sum_{\substack{i,j,v \in V \\ i \neq j \neq v}} \frac{g_{ij}(v)}{g_{ij}}$$

where $g_{ij}$ is the number of shortest paths going from node *i* to *j*, *i* and $j \in V$ and $g_{ij}(v)$ the number of shortest paths from *i* to *j* that pass through the node *v*.

Statistical significance for the interconnectivity of MV-V interactors was assessed by a random resampling testing procedure ($n$ = 10,000 permutations). For each permutation, we randomly extracted a list of proteins equal in size to the MV-V interactor list from the human interactome, and the number of shared interactions was assessed. The randomization procedure was weighted and corrected according to the connectivity of proteins in order to prevent inspection bias on highly studied proteins. A theoretical distribution was computed for the 10,000 resampled values. From this distribution, an empirical *p* value was computed by counting the number of resampled values greater than the value observed for MV-V interactors.

Statistical significance for the number of proteins targeted by at least one viral protein was evaluated by comparison with the distribution obtained by random simulation using R. We randomly drew as many proteins as those identified as MV-V interactors from the human proteome, and we numbered the number of proteins targeted by at least one viral protein. This procedure was repeated 10,000 times. From this distribution, an empirical *p* value was computed by counting the number of resampled values greater than the value observed for MV-V interactors.

*siRNA-Mediated Histone Deacetylase Complex Down-Regulation*—Synthetic double-stranded siRNA were purchased from Applied Biosystems (Catalog numbers: s17391, s17629, s11847, s2984, s28737, s224320, s223571, s10457) to knock-down the expression of MTA1, MTA2, RBBP7, CHD4, MBD3, GATAD2A, ZBTB43 (CT1), and PDK2 (CT2), respectively. A standard protocol of forward siRNA transfection was used. One day before transfection HEK-293T cells were plated in either 96-well white microplates (for subsequent luciferase and cell viability assays) or in 96-well transparent microplates (for Imaging). In each well $2 \times 10^4$ cells were seeded in 0.08 ml DMEM medium with 10% fetal bovine serum, but without antibiotics . Transfections with siRNAs were carried out in triplicate the next day using Lipofectamine RNAi-MAX (Invitrogen) according to the manufacturers' protocol. For each well 6 pmol siRNA and 0.25 $\mu$l RNAi-MAX transfection reagent combined with 20 $\mu$l of Opti-MEM serum-free medium (Invitrogen) were added. At 24 h post-transfection cells were infected with recombinant MVs expressing Luc or CH proteins (rMV2/Luc or rMV2/STrEP-CH) at an MOI of 0.5, or mock-treated to determine cell viability. For recombinant MV expressing Luc, luciferase activity was determined 48 h postinfection using the Bright-Glo Luciferase assay system (Promega). Cell viability was determined at the same time-point using the CellTiter-Glo Luminescent Cell Viability Assay (Promega). Luminescence was measured using a 2300 EnSpire Multilable Plate reader (PerkinElmer). Fluorescent and light microscopy was performed 48 h postinfection with rMV2/STrEP-CH to determine CH protein expression levels and cell-to-cell fusion events in siRNA-transfected HEK-293T cells.

*Inhibition of Histone Deacetylase Activity with Trichostatin A (TSA)*—In each well $4 \times 10^4$ cells were plated in either 96-well white microplates (for subsequent luciferase and cell viability assays) or in 96-well transparent microplates (for Imaging). The next day, cells were treated or not with TSA (Sigma, dose range from 1 to 0.06 $\mu$M), and infected with recombinant rMV2/Luc or rMV2/STrEP-CH at an MOI of 0.2 or mock-treated to determine cell viability. These experiments were carried out in duplicates. Luciferase assays were performed as described above 48 h postinfection or 48 h after TSA treatment. Fluorescent and light microscopy was performed 72 h postinfection with rMV2/STrEP-CH to determine CH protein expression level in HEK-293T cells in the presence or absence of TSA.

*Fluorescence Microscopy Imaging*—Fluorescence corresponding to the mCherry reporter (excitation/emission: 587/610 nm) was observed using the DM IRB inverted research microscope (Leica) supplied with the green filter N2.1 (Leica; BP 515–560 nm) and imaging was performed using the QImaging *Retiga EXi Fast 1394* CCD camera.

## RESULTS

*Generation of Recombinant MV Expressing a Tagged MV-V*—To copurify MV-V with associated protein complexes from infected cells, MV-V has to be expressed from MV genome with a fusion tag allowing its capture. To reach this goal, we took advantage of a reverse genetic system for MV based on the Schwarz vaccine strain that has been developed in our lab (20). A sequence encoding for MV-V protein with an amino-terminal One-STrEP tag was inserted into the pTM-Schw plasmid containing MV genome, in an additional transcription unit located downstream of the P gene (Fig. 1). According to previous studies, known MV-V functions are not affected by the addition of an amino-terminal tag (14, 15, 17, 32). The engineered recombinant virus was designated rMV2/STrEP-V. As a negative control, we also produced a recombinant virus expressing the CH protein instead of MV-V (designated rMV2/STrEP-CH). In each construct, a flexible TEV protease coding linker was inserted between the One-STrEP tag and MV-V or CH proteins to provide a strategy for releasing protein complexes after purification. Recombinant viruses encoding One-STrEP-tagged MV-V or CH proteins were successfully rescued by transfecting the rMV2/STrEP-V and rMV2/STrEP-CH plasmids into helper cells and propagation on Vero cells as previously described (20, 21).

*Recombinant Viruses Properly Express Tagged MV-V and CH Proteins, and Replicate at High Titers*—To detect the expression of MV-V and CH-tagged proteins from rMV2/STrEP-V and rMV2/STrEP-CH, Vero cells were infected with recombinant viruses, and protein expression was determined 24 h postinfection by Western blot analysis. High levels of tagged MV-V and CH proteins were detected in infected cells (Fig. 2*A*). In rMV2/STrEP-V infected cells, a second One-STrEP-tagged protein with a lower molecular weight than One-STrEP-tagged MV-V was also detected by Streptavidin-HRP blotting. This protein is most likely produced from One-STrEP-tagged MV-V encoding mRNA molecules where one additional nontemplated guanine nucleotide has been inserted by the viral polymerase at the editing site (33). This

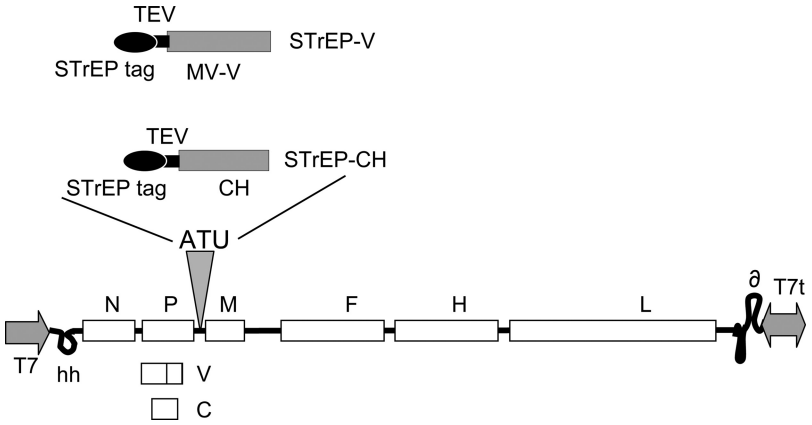


FIG. 1. **Schematic representation of recombinant virus genomes.** MV negative-sense RNA genome is displayed with its 3′ end on the *left*, with the six genes indicated by capital letters and depicted as white rectangles. The additional transcriptional units encoding for One-STrEP-tagged MV-V (STrEP-V) or CH protein (STrEP-CH) are inserted between P and M genes. The black oval represents the One-STrEP-tag sequence and the black rectangle corresponds to the Tobacco Etch Virus (TEV) protease coding linker. T7p is a T7 RNA polymerase promoter sequence, hh is a hammerhead ribozyme, T7t is a T7 RNA Polymerase termination signal, ∂ is a hepatitis delta ribozyme.

results in a truncated MV-V protein encompassing the amino-terminal PNT region plus five specific C-terminal amino acids. CH expression from rMV2/STrEP-CH was also assessed by fluorescent microscopy (Fig. 2B). Altogether, this demonstrates that additional transcriptional units within rMV2/STrEP-V and rMV2/STrEP-CH are properly expressed.

We also tested the potential impact of such additional transcriptional units on viral replication by determining single-step growth curves of rMV2/STrEP-V and rMV2/STrEP-CH viruses on Vero cells (Fig. 2*C*). The growth of recombinant viruses was similar to that of unmodified MV (Schwarz), and titers were comparable. In conclusion, both recombinant viruses efficiently propagated through the cell monolayer, with no detectable interference with viral replication, and properly expressed tagged MV-V or CH proteins.

*Purification of MV-V and Associated Protein Complexes*—The whole purification protocol is presented as a flow chart in Fig. 3. The MV-V protein was copurified together with its cellular interacting partners from HEK-293T cells infected with rMV2/STrEP-V recombinant virus at an MOI of 1. One-STrEP-tagged MV-V protein and associated cellular factors were isolated from total cell extracts collected 24 h postinfection by single-step affinity purification using Strep-Tactin Sepharose beads. MV-V and interacting partners were subsequently released from the beads by TEV cleavage and protein samples were resolved by SDS-PAGE electrophoresis (Fig. 4*A*). Many proteins were copurified with MV-V, whereas in contrast, only a limited number of proteins were copurified with CH from the rMV2/STrEP-CH negative control. Most importantly, we confirmed that two well-characterized MV-V binding partners, STAT1 and STAT2, were detected among cellular proteins that copurified with STrEP-V but not STrEP-CH (Fig. 4*A lower* panel). Thus, protein samples were analyzed directly by nano-LC-MS/MS, without the need to separate proteins by SDS-PAGE electrophoresis and perform in-gel digestions.

*Identification of Virus-Host Protein Partners by MS*—To obtain a comprehensive list of both direct and indirect interactors of MV-V protein, HEK-293T cells were infected with either rMV2/STrEP-V or rMV2/STrEP-CH at an MOI of 1. Tagged MV-V or CH proteins were purified 24 h postinfection by the affinity chromatography procedure presented above, and co-purified cellular proteins were directly identified by nano-LC-MS/MS analysis. The same experiment was repeated three times, and only cellular proteins that were copurified with MV-V but never found in association with the control CH protein were considered (Fig. 4*B* and supplemental Table S1). Interestingly, we found large overlaps between all three experiments, thus demonstrating the robustness of this experimental approach. A list of 245 unique MV-V partners was generated that contains only cellular proteins found at least in two independent experiments (supplemental Table S2). Within this list, best-known direct interactors of MV-V were identified, including STAT1, STAT2, and IFIH1, confirming the sensitivity of this method. We also found p53 that was previously reported to interact directly with the C-terminal VCT region of MV-V (19). In contrast, we failed to identify five known interactors of MV-V: p73, LGP2, IKK-$\alpha$, IRF7, or JAK1. A weak expression in HEK-293T cells (*e.g.* IRF7) or a strong association with membrane-associated receptors (*e.g.* JAK1) could explain their absence from this data set. Altogether, these data show that our mapping strategy is sensitive, and provides reproducible data.

*Specificity of Our Virus-Host Protein Mapping Approach*—Bait-prey interactions identified using our approach represents both direct and indirect interactors of MV-V protein. In addition to cellular partners, MV-V was also found to interact with viral proteins, in particular MV nucleoprotein N (MV-N, supplemental Table S3). This interaction has been previously reported, and is mediated by the N-terminal PNT region of MV-V (34). This suggests that some of the 245 cellular pro-

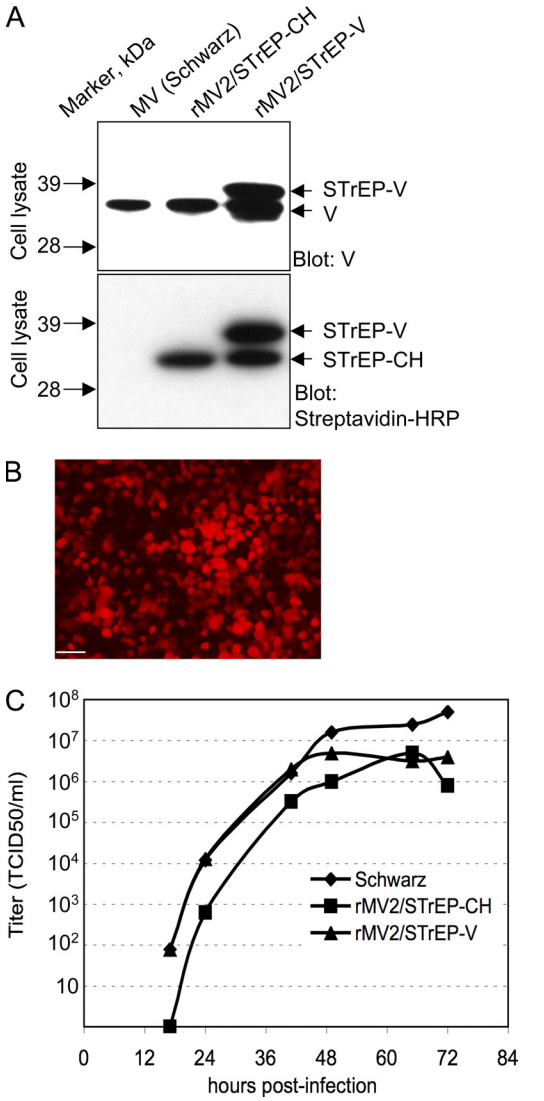


FIG. 2. **Characterization of recombinant viruses expressing STrEP-V or STrEP-CH proteins.** *A,* Vero cells were infected with the native MV Schwarz strain, or the rMV2/STrEP-CH expressing the One-STrEP-tagged CH protein, or the rMV2/STrEP-V expressing the One-STrEP-tagged MV-V protein. Expression of native and One-STrEP-tagged MV-V proteins was determined by Western blot using anti-V monoclonal antibodies (*top* panel). Expression of One-STrEP-tagged CH or MV-V proteins was determined by Western blot using Streptavidin-HRP conjugates (*lower* panel). *B*, Fluorescent microscopy showing efficiency of CH protein expression in HEK293T 24 h postinfection by rMV2/STrEP-CH. Fluorescence images were taken with a 10 × objective. White scale bar correspond to 100 $\mu$m. *C*, Single-step growth curves obtained for rMV2/STrEP-V and rMV2/STrEP-CH. MV Schwarz strain was used as a control. Vero cells in 6-well dishes were infected with MV Schwarz, rMV2/STrEP-V, or rMV2/STrEP-CH at an MOI of 0.1. Cell-associated virions were recovered at each time point, and titers were determined using the TCID50 method.

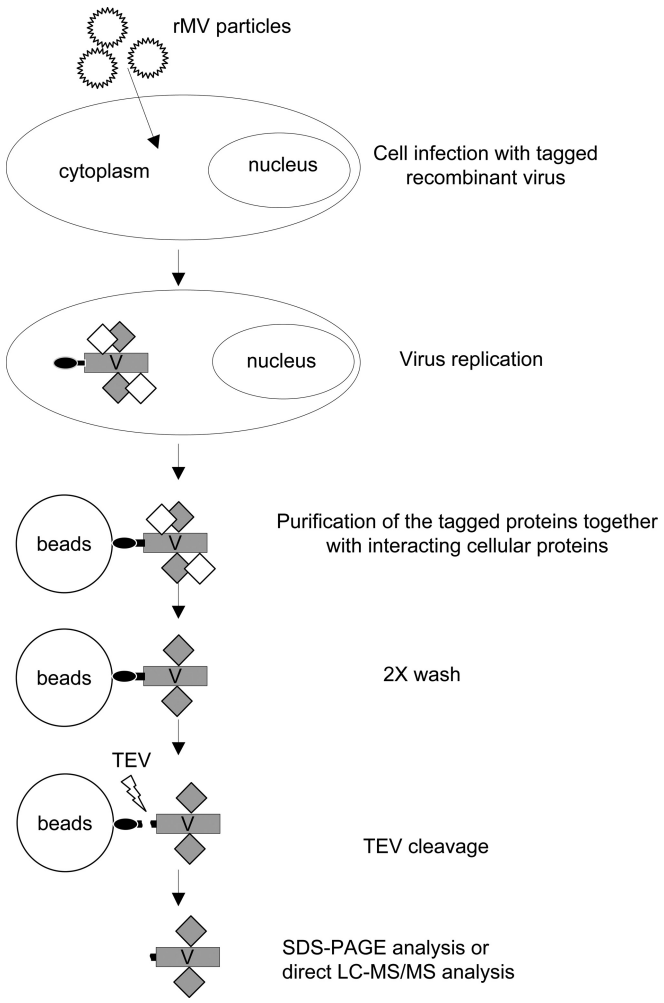


FIG. 3. **Summary of the protocol used to purify STrEP-V and associated cellular proteins from infected cell lysates.** HEK-293T cells were infected with rMV2/STrEP-V or rMV2/STrEP-CH at an MOI of 1. 24 h postinfection, STrEP-V was copurified with interacting cellular proteins using StrepTactin Sepharose beads. After two subsequent washing steps, protein complexes were released from the beads by specific cleavage of a flexible linker by the TEV protease. Protein complexes were precipitated and quantified. Finally, purified virus-host protein complexes were analyzed by direct nano-LC-MS/MS. White circles represent StrepTactin Sepharose beads, white rhombus represent unbound proteins and contaminants, and gray rhombus correspond to MV-V interacting partners. A white lightning indicates the cleavage site for the TEV protease. Other indications are as in Fig. 1.

teins copurified with MV-V could be indirect interactions mediated by N as a bridge. To address this question, we engineered a new virus expressing the MV-N protein with a One-STrEP C-terminal tag (designated rMV2/N-STrEP). Previous reports have demonstrated that known MV-N functions are not affected by the addition of C-terminal tag (35). As a negative control, we also produced a recombinant virus expressing the CH protein with a C-terminal tag (designated rMV2/CH-STrEP) (Fig. 5*A*). The expression of tagged MV-N and CH proteins was validated by Western blot (Fig. 5*B*). Recombinant rMV2/N-STrEP and rMV2/CH-STrEP were also shown to replicate at high titers (Fig. 5*C*). HEK-293T cells were infected as described above with rMV2/N-STrEP or

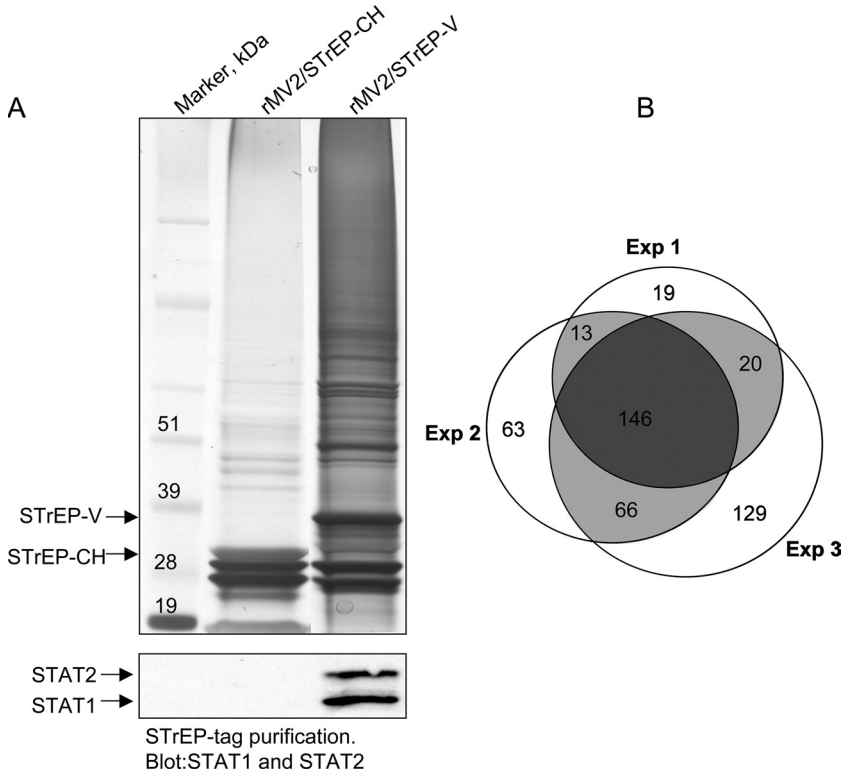


FIG. 4. **Purified protein complex analysis.** *A*, Purified protein complexes were resolved by SDS-PAGE and silver staining (*top* panel). Same protein samples were resolved by SDS-PAGE followed by Western blot analysis to detect MV-V interactions with STAT1 and STAT2 proteins (*lower* panel). *B*, Venn diagram showing overlaps between three lists of MV-V interacting partners established from three independent experiments. For each experiment, a negative control was obtained by processing rMV2/STrEP-CH infected cells. Any host protein that copurified with STrEP-CH in at least one of the three experiments was systematically discarded from the list of MV-V interacting partners. A list of MV-V interacting partners that contains 245 cellular proteins was established from the overlap between at least two independent experiments.

rMV2/CH-STrEP viruses, and copurified protein complexes were similarly analyzed. Protein profiles obtained by SDS-PAGE electrophoresis were obviously different from those observed with MV-V with only few copurified proteins specific of MV-N (Fig. 5*D*). This result was confirmed by nano-LC-MS/MS analysis where only eight unique cellular partners were identified for MV-N (supplemental Table S4 and S5) and only two of them were in the list of the unique MV-V interactors (Fig. 5*E*). Altogether, this demonstrates that most of MV-V partners, which can be either direct or indirect interactors, are highly specific of this viral protein because they were not identified with MV-N in a parallel experiment.

*Specificity of MV-V Protein Interaction With Cellular Partners in the Absence of Viral Replication*—To determine if the interactions reported above between MV-V and host proteins are dependent on the micro-environment induced by MV infection, we expressed the STrEP-V protein alone in HEK-293T cells and characterized its binding partners by affinity chromatography and MS analysis. In addition, full-length MV-V and the PNT region alone were compared for their ability to bind cellular partners, because this N-terminal MV-V fragment is intrinsically disordered and thus potentially responsible for interactions with multiple protein partners (36, 37). We generated plasmids encoding for full-length MV-V or its PNT region alone fused to the amino-terminal One-STrEP tag (designated pCI-neo/STrEP-V or pCI-neo/STrEP-PNT, Fig. 6*A*). As a negative control, we also produced a plasmid encoding for a One-STrEP-tagged CH protein (designated pCI-neo/CH-STrEP). These plasmids were transiently transfected in HEK-293T cells. Then, MV-V and PNT protein complexes were isolated from total cell extracts collected 24 h post-transfection, and the single-step affinity purification was performed as described above. Protein profiles obtained by SDS-PAGE electrophoresis for MV-V and PNT copurified protein complexes differed from one another (Fig. 6*B*). Many proteins were copurified with MV-V, but only a limited number of cellular proteins were copurified with the PNT region alone or the CH-STrEP negative control (Fig. 6*B*). Using nano-LC-MS/MS analysis, two lists of cellular binding partners were established, where only cellular proteins that were copurified with either MV-V or PNT but not found in association with the control CH protein were considered (supplemental Table S6). In total, 323 cellular proteins were found to copurify with MV-V when expressed alone by transient transfection. This list was compared with the list of 245 MV-V partners generated in the viral context (Fig. 6*C* and supplemental Table S7). A large overlap was observed between the two lists, with 57.9% of the interactions recovered from MV-infected cells that were also found when expressing MV-V alone. These results show a strong correlation between the two interactions lists, supporting the fact that most interactions detected in MV-infected cells are dependent on MV-V protein expression alone. Interestingly, only 20 interactions were identified with the PNT region alone, and most of them were common to full-length MV-V. STAT1 was detected among cellular proteins that copurified with both STrEP-V and STrEP-PNT, thus confirming our previous results showing that the PNT region is responsible for the direct MV-V interaction with STAT1 (15, 17).

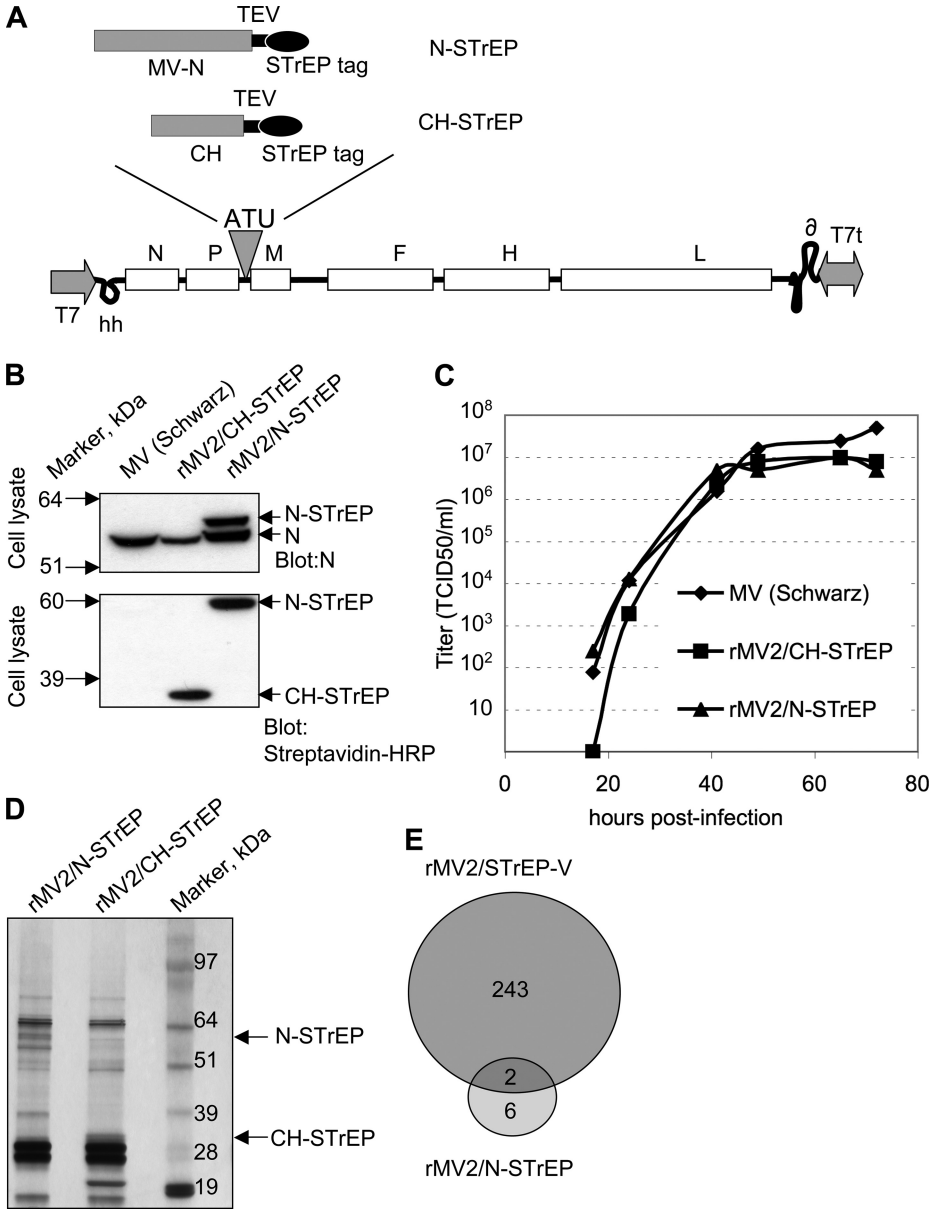


FIG. 5. **MV-V and MV-N exhibit very distinct lists of cellular binding partners.** *A*, Schematic representation of rMV2/N-STrEP and rMV2/CH-STrEP genomes that encode for MV-N and CH with a C-terminal One-STrEP tag (N-STrEP and CH-STrEP, respectively). *B*, N-STrEP and CH-STrEP expression was validated by Western blot using anti-N antibodies or Streptavidin-HRP conjugates. *C*, Single-step growth curves of rMV2/N-STrEP and rMV2/CH-STrEP. *D*, Purified protein complexes analysis for N-STrEP and CH-STrEP by SDS-PAGE followed by silver staining. *E*, Overlap between protein sets identified as MV-V or MV-N interacting partners.

These results further support the high specificity of our purification strategy because only the full-length MV-V protein, and not its N-terminal PNT domain expressed in the same condition outcome in a large list of cellular partners. They also demonstrate that the C-terminal region plays a critical role in MV-V ability to form large complexes with numerous host factors.

*Functional Analysis of MV-V Interaction Network*—We then analyzed MV-V cellular interactors for functional enrichment using protein interaction databases, Gene Ontology annotation, and the literature. We first performed a query on protein interaction databases using APID2NET search tool (26). The 245 human cellular proteins that copurified with MV-V were found connected by no less than 766 protein-protein interactions. This interactome network was displayed using Cytoscape application (Fig. 7), and exhibits a core component of 147 cellular proteins, whereas 98 proteins were either isolated from the core component (79 proteins) or simply not referenced in APID2NET (19 proteins). We then analyzed this network for functional enrichment using Gene Ontology (GO) database and BINGO2 plugin for Cytoscape (28, 29). As expected and because of MV-V binding to STAT1, STAT2, IFIH1, and p53, this network was statistically enriched for cellular components involved in "response to biotic stimulus," a GO term encompassing cellular "response to viruses." A significant enrichment was also detected for protein chaperones, suggesting that MV-V triggers an unfolded protein response upon accumulation in infected cells. More surprisingly, MV-V infection network was also enriched for several components of the histone deacetylase complex, suggesting yet uncharacterized

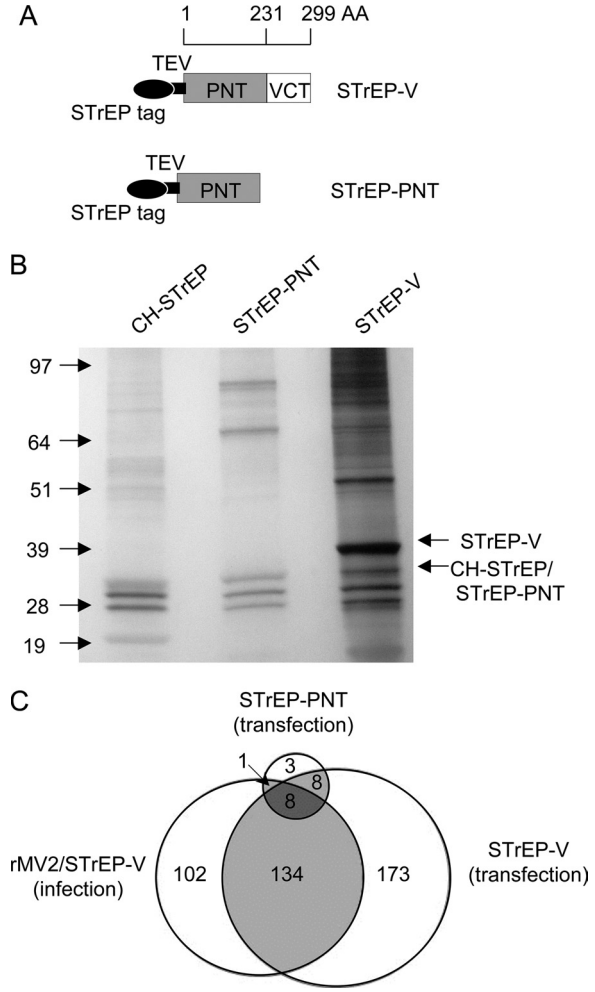


FIG. 6. **Specificity of MV-V interaction with cellular partners in the absence of viral replication.** *A*, Schematic representation of One-STrEP tagged full-length MV-V and MV-PNT domain used for cloning in pCI-neo. *B*, Purified protein complexes analysis of transiently expressed in HEK-293T cells STrEP-V, STrEP-PNT, and CH-STrEP proteins by SDS-PAGE followed by silver staining. *C*, Venn diagram showing overlaps between cellular protein sets identified as interacting partners of the full length MV-V and PNT domain in the absence of infectious context and the 245 cellular partners of the full-length MV-V protein identified in an infectious context.

acterized interactions with chromatin remodeling and gene silencing machineries. Interactions with multiple components of the protein phosphatase 2A complex also suggest MV-V implications in serine/threonine kinase signaling pathways. Interestingly, this latter interaction was recently confirmed by yeast two-hybrid approach (Caignard, G. et al., manuscript in preparation), thus demonstrating MV-V direct binding to protein phosphatase 2A. The MV-V infection network was highly enriched for mitochondria, reticulum, and ribosomal proteins. Although this unravels close interactions between these cellular components and MV-V, functional consequences on the virus replication cycle will require further investigations. Importantly, the profile of cellular modules that copurified with MV-V was highly conserved, whether this viral protein was expressed from MV genome in infected cells or by transient transfection of plasmid DNA (compare Fig. 7 and Fig. 8). Thus, MV-V alone has the capacity to interact with these different functional modules, independently of other viral factors.

*Topological Analysis of MV-V Interaction Network*—We then analyzed the MV-V infection network for specific topological features. First, we asked whether host proteins that copurified with MV-V are central in the human interactome network. Local (degree) and global (betweenness) centrality measures were calculated. Briefly, the degree ($k$) of a protein in a network corresponds to its number of direct partners and is therefore a measure of local centrality. Betweenness ($b$) is a global measure of centrality, as it measures the number of shortest paths (the minimum distance between two proteins in the network) that pass through a given protein. The degree distribution of cellular proteins copurified with MV-V was plotted, and compared with the distribution obtained for the whole human interactome network (Fig. 9*A*). These distributions were significantly distinct ($U$ test; $p$ value $< 2.2 \times 10^{-16}$), and MV-V cellular interactors showed an average degree ($k = 21.19$) that is much higher than the average degree of cellular proteins in the human interactome ($k = 7.39$). Thus, cellular proteins that copurified with MV-V exhibit much more cellular partners than normally expected by chance. We also calculated and plotted the betweenness centrality distribution for the cellular proteins that copurified with MV-V (Fig. 9*B*). This distribution was significantly different from the one obtained for the whole human interactome network ($U$ test; $p$ value $< 2.2 \times 10^{-16}$), and MV-V cellular interactors showed an average betweenness centrality coefficient ($b = 3.64 \times 10^{-4}$) that is much higher than the average betweenness centrality coefficient of cellular proteins in the human interactome ($b = 1.06 \times 10^{-4}$). Thus, betweenness centrality measures show that MV-V interacting partners are enriched for vertices that connect multiple modules in the human interactome. Furthermore, MV-V interacting proteins are highly interconnected, because they share 2.5 more interactions than expected for a random protein set (Fig. 9*C*; $p$ value $< 1 \times 10^{-5}$). Thus, MV-V interacting proteins correspond to well-defined functional modules composed of large protein complexes. This conclusion is clearly in agreement with the GO term analysis described above where MV-V is shown to target cellular organelles like mitochondria or multiprotein complexes like ribosomes, histone deacetylases, or protein phosphatase 2A. Altogether, topological analyses of MV-V interaction network demonstrate that MV-V preferentially interacts, either directly or indirectly, with host proteins that are central in the human interactome network, and represent well-defined functional modules as assessed by the enrichment for proteins sharing interactions. This is clearly in the line of previous reports showing that viral proteins preferentially bind host proteins with such characteristics (2, 3, 38, 39).

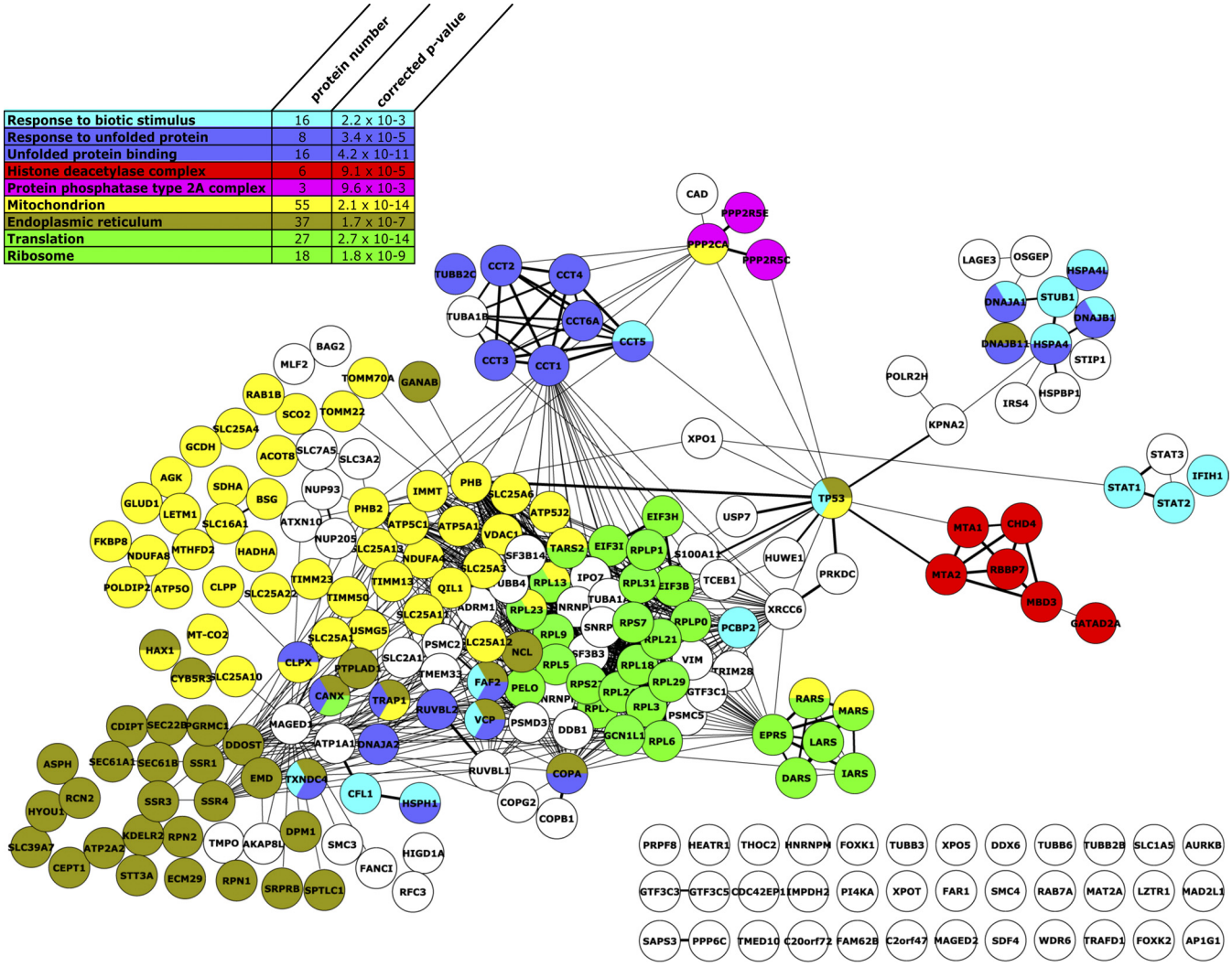


FIG. 7. **A map of the human protein interaction subnetwork targeted by MV-V.** From the list of cellular interactors of MV-V in infected cells identified by nano-LC-MS/MS analysis, we queried interaction databases using APID2NET search tool. Retrieved interactions were displayed using Cytoscape network analysis tool. Statistical enrichment for specific GO terms was determined using BINGO2 plug-in. A selection of statistically significant GO terms ($p$ value $< 0.01$) was displayed on the map by coloring the corresponding nodes with GOlorize plug-in.

*MV-V Interactors Are Well-known Targets of Viruses in General*—We thus queried the VirHostNet database using our list of MV-V interactors, and identified a total of 220 distinct virus-host interactions involving 50 different virus species. Of the 245 cellular proteins that copurified with MV-V, 44.9% correspond to known targets of at least one other virus (110 out of 245, see Fig. 9*D* and supplemental Table S8). This corresponds to a strong enrichment when compared with the 5.4% of human proteins identified as viral targets in VirHostNet. Statistical significance was assessed by Fisher's exact test ($p$ value $< 2.2 \times 10^{-16}$), but also by comparing our dataset with 10,000 random sets of 245 human proteins ($p$ value $< 1 \times 10^{-5}$; Fig. 9*D*). This demonstrates that MV-V cellular targets mostly correspond to host factors that are critical to viral replication in general, and thus represent common targets for several viruses. Most importantly, this clearly provides a strong argument to support the quality of our MV-V infection network obtained using a combination of reverse genetic with proteomic analysis.

*Functional Evidence of MV-V Interaction with Histone Deacetylase Complex Proteins*—MV-V interaction with cellular translational machinery and mitochondria proteins is not surprising because many viruses hijack these cellular machineries to achieve successful replication. However, we were more surprised by the enrichment of MV-V infection network for several histone deacetylase complex proteins (HDAC). As a proof of concept for the functional validation of this virus-host interaction map built in a viral context, we examined a potential role of HDACs in MV replication. First, we engineered a recombinant virus expressing the firefly luciferase protein

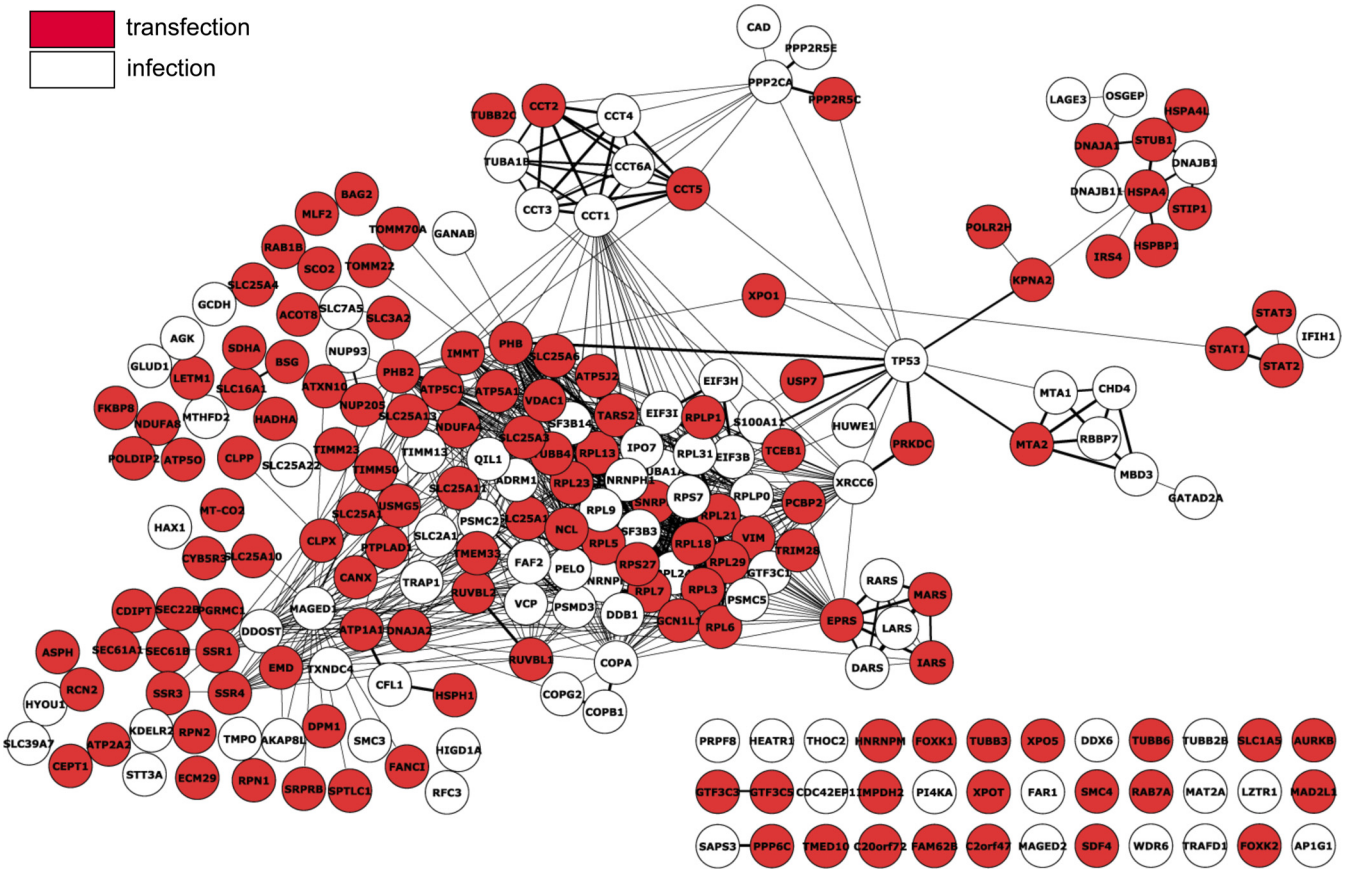


FIG. 8. **A map depicturing an overlap of two human protein interaction subnetworks targeted by MV-V in the presence or absence of viral infection.** The same as on Fig. 7 but 142 cellular proteins found to interact with MV-V in the absence of viral background are shown in red and represent a large overlap between MV-V interactors recovered in the presence and absence of viral infection.

(Luc) in the additional transcription unit between MV-P and MV-M proteins. This virus was designated rMV2/Luc and expressed Luc when replicating in target cells. Then, HEK-293T cells were infected with rMV2/Luc at an MOI of 0.2 in the absence or presence of inhibitor of histone deacetylase activity Trichostatin A (TSA). Treatment with TSA increased MV replication in a dose-dependent manner as assessed by Luc expression (3.2-fold increase with 1 $\mu$M of TSA; Fig. 11*A*), despite a substantial effect on cell viability at highest TSA concentrations (supplemental Fig. S3). MV replication in the presence or absence of TSA was also assessed by fluorescent microscopy using the rMV2/STrEP-CH recombinant virus (supplemental Fig. S4). TSA treatment increased CH expression, and much larger virus-induced syncytia were observed. Thus, the HDAC inhibitor TSA increased MV replication in target cells.

Metastasis-associated proteins (MTA1 and MTA2), Chromodomain-helicase-DNA-binding protein 4 (CHD4 or Mi2-beta), Histone-binding protein (RBBP7), Methyl-CpG-binding domain protein 3 (MBD3), and Transcriptional repressor p66-alpha (GATAD 2A) are six HDAC components found to interact with MV-V protein in an infectious context (Fig. 7, supplemental Table S2). To further support the biological relevance of these interactions, we knocked-down these proteins and then determined MV replication. HEK-293T cells were transfected with MTA1, MTA2, CHD4, RBBP7, MBD3, or GATAD2A-specific siRNAs, or control siRNAs (CT1 and CT2). Transfected cells were cultured for 24h, infected with rMV2/Luc (MOI 0.5), and then lysed 48 h postinfection. Transfection of these different siRNAs had no effect on cell viability (supplemental Fig. S5). Silencing of RBBP7, MBD3, GATAD2A positively regulated MV replication as assessed by luciferase expression (Fig. 11*B*). These results were confirmed by fluorescent microscopy when using rMV2/STrEP-CH to infect HEK-293T cells. Higher expression levels of CH protein and larger syncytia were observed in cells where RBBP7 or GATAD2A expression was suppressed (Fig. 11*C*). Thus, siRNA-mediated silencing of HDAC components that are specific MV-V interactors enhances MV replication, suggesting a negative role of deacetylation on viral replication.

## DISCUSSION

To map virus-host protein interactions, we developed a new method based on recombinant viruses expressing tagged viral proteins to capture their physical binding partners during infection. More specifically, a reverse genetic system was

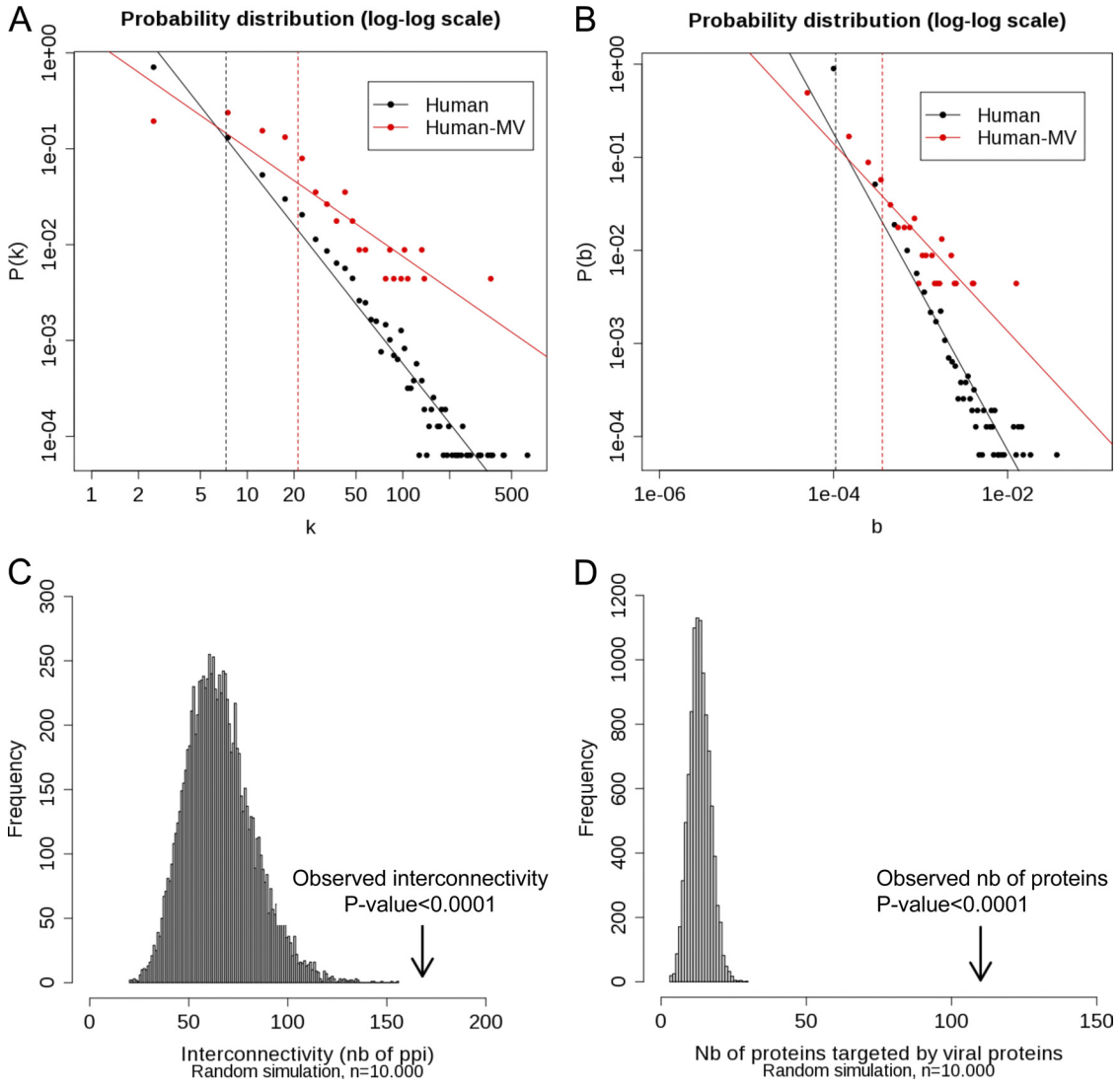


FIG. 9. **Topological analysis of MV-V infection network.** *A*, Degree and *B*, betweenness distributions of human proteins (black) and human proteins copurified by MV-V (red) in the human interactome. P(k) is the probability of a node to connect k other nodes in the network. P(b) is the probability of a node to have a betweenness equal to b in the network. Solid lines represent the linear regressions. Vertical dashed lines correspond to mean degree and betweenness values. *C*, Human proteins copurified with MV-V are highly interconnected. Protein sets were randomly drawn from the human proteome, and protein-protein interactions in the corresponding subgraph were numbered. This was repeated 10,000 times before plotting the observed distribution. The value observed with the set of proteins that copurified with MV-V (168 interactions) is indicated by a vertical arrow, and demonstrates a statistically significant enrichment for highly interconnected cellular proteins. *D*, Cellular proteins interacting with MV-V are preferential targets of viruses. Protein sets were randomly drawn from the human proteome, and the number of proteins targeted by at least a viral protein was determined. This was repeated 10,000 times, and the corresponding distribution was plotted. The value observed with the set of proteins that copurified with MV-V (110 cellular proteins targeted by at least one virus) is indicated by a vertical arrow, and demonstrates a statistically significant enrichment for cellular proteins that represent frequent targets for viruses in general.

used to engineer MV genome, and rescue virus strains that encode for tagged MV-V or MV-N proteins. This allowed virus-host protein complex analysis directly from infected cells by combining modified tandem affinity chromatography and mass spectrometry analysis. Our modified One-STrEP tag protocol resulted in highly purified protein complexes compatible with a direct analysis of their components by nano-LC-MS/MS. Most importantly, we show that reproducible lists of cellular partners were obtained with this approach as assessed by convergent results obtained from three biological replicates. Finally, we established a list of 245 direct or indirect binding partners for MV-V, providing new hypothesis to investigate the biology of this virus (supplemental Table S2).

Among the 245 cellular proteins that copurified with MV-V, we were able to recover four of the nine cellular proteins previously described as direct binding partners of this virulence factor, including STAT1, STAT2, IFIH1, and p53. Until

now, these interactions were essentially documented in cells transiently or stably transfected with MV-V (15, 17–19, 40, 41). To our knowledge, this is the first report demonstrating that all these interactions actually occur in MV-infected cells, in highly relevant conditions where MV-V is encoded by the viral genome itself. Finding previously described interactions nicely supports the relevance of our system. However, we did not recover all previously reported interactions, but this could be explained by technical or biological limitations. Indeed, some previously reported interactions could be too unstable to withstand the stringent conditions that were used to purify MV-V complexes. In addition, some cellular proteins with unusual physical properties can be difficult to detect by MS analysis. Finally, some interactions could only occur in specific cell types or culture conditions but we should be able to address this point in the future. Indeed, our approach is suitable to probe viral protein partners in different cell types or culture conditions all along a virus replication cycle. This represents a major advantage of our strategy and in the future, we should be able to identify interactions that only occur in specific cell types, culture conditions, or infected tissues. We could even use the same strategy to investigate virus-host protein interactions directly *in vivo* by processing tissue samples from infected animals.

In addition to previously reported interactions, our strategy led to identify a prosperous list of 245 cellular proteins that copurified with MV-V (supplemental Table S2). Although MV-V exhibits a large intrinsically disordered N-terminal region that could favor direct binding to numerous partners (for review see (37), most of the interactions identified are likely to be indirect. Indeed, our interaction mapping strategy does not discriminate between direct and indirect protein-protein interactions. In the future, our approach should be combined with other technologies that essentially detect binary protein-protein interactions like Nucleic Acid Programmable Protein Array, Luminescence-based Mammalian IntERactome, Mammalian Protein-Protein Interaction Trap, or Protein Complementation Assay (for review see (42).

Strong bioinformatic and experimental arguments support the high relevance of our list of MV-V interactors. First and as aforementioned, this list of 245 cellular proteins was based on the overlap of at least two out of three biological replicates, and thus corresponds to reproducible interaction data. In addition, host proteins that copurified with CH protein from control viruses were systematically discarded to eliminate sticky proteins and potential false positives. To further establish the specificity of our MV-V interactor list, we also built a recombinant virus expressing MV-N with a One-STrEP tag. In the same experimental conditions that were applied to identify MV-V binding partners, only eight cellular proteins copurified with MV-N. Interestingly, only two cellular proteins interacted both with MV-N and MV-V (Fig. 5*E*, supplemental Table S5). This is not surprising because MV-V was previously reported to interact with MV-N *via* its N-terminal PNT region (34), and this is confirmed by the presence of MV-N in protein complexes copurified with MV-V (supplemental Table S3). We also established that a majority of cellular proteins that copurified with MV-V in infected cells also copurified with this viral protein when expressed by transient transfection, whereas only a minor subset was copurified when expressing the PNT region of MV-V alone (Fig. 6*C* and supplemental Table S7). This demonstrates that our list of MV-V binding partners, although it clearly corresponds both to direct and indirect interactions, is highly specific of this viral protein.

Statistical analyses also support the high relevance of our list of MV-V interactors. Indeed, cellular proteins that copurified with MV-V are significantly enriched for central proteins with high connectivity and betweenness coefficients, and exhibit strong interconnections in the human interactome network (Fig. 9). These topological features are clearly distinct from those obtained by random sampling, thus demonstrating that our list of MV-V interactors is skewed for host proteins exhibiting specific characteristics. Furthermore, this topological bias was previously reported in other studies that aimed at mapping virus-host protein interactions in a large-scale setting (2, 3, 39). Indeed, viral proteins in general have strong tendency to target host proteins that are central in the human interactome network, and represent key components of essential cellular modules as assessed by their topological features. As a corollary, we found that a large fraction MV-V interacting partners correspond to known targets of other viruses (Fig. 10 and supplemental Table S8). Again, this strong enrichment nicely confirms the relevance of our strategy, and supports the idea that MV-V binds directly or indirectly to a kernel of cellular complexes that are hijacked by most, if not all, viruses.

In addition to previously reported interactions with key components of the host antiviral response including STAT1, STAT2, IFIH1, and p53, MV-V was found to target essential components of ribosomes, reticulum, and mitochondria. As part of the protein synthesis machinery, we identified a set of ribosomal proteins, translation factors, chaperones, and aminoacyl-tRNA synthetases among MV-V associated proteins (Fig. 7 and supplemental Table S2). These host proteins might be recruited by MV-V to optimize translation of nascent viral mRNA molecules. Conversely, interactions with host translation machinery could prevent the synthesis of antiviral factors of which expression is controlled at translational level (43). MV-V interactions with endoplasmic reticulum components is also new, and could participate in the processing, maturation, and transport of viral proteins from perinuclear regions to the cell surface. The enrichment for mitochondrial proteins is also very important. For the moment, the role of mitochondria in the replication cycle of nonsegmented negative-strand RNA viruses is less well studied than for positive-stranded RNA viruses. We identified numerous components of mitochondrial protein precursors import complex (TOM, TIM, VDAC), solute

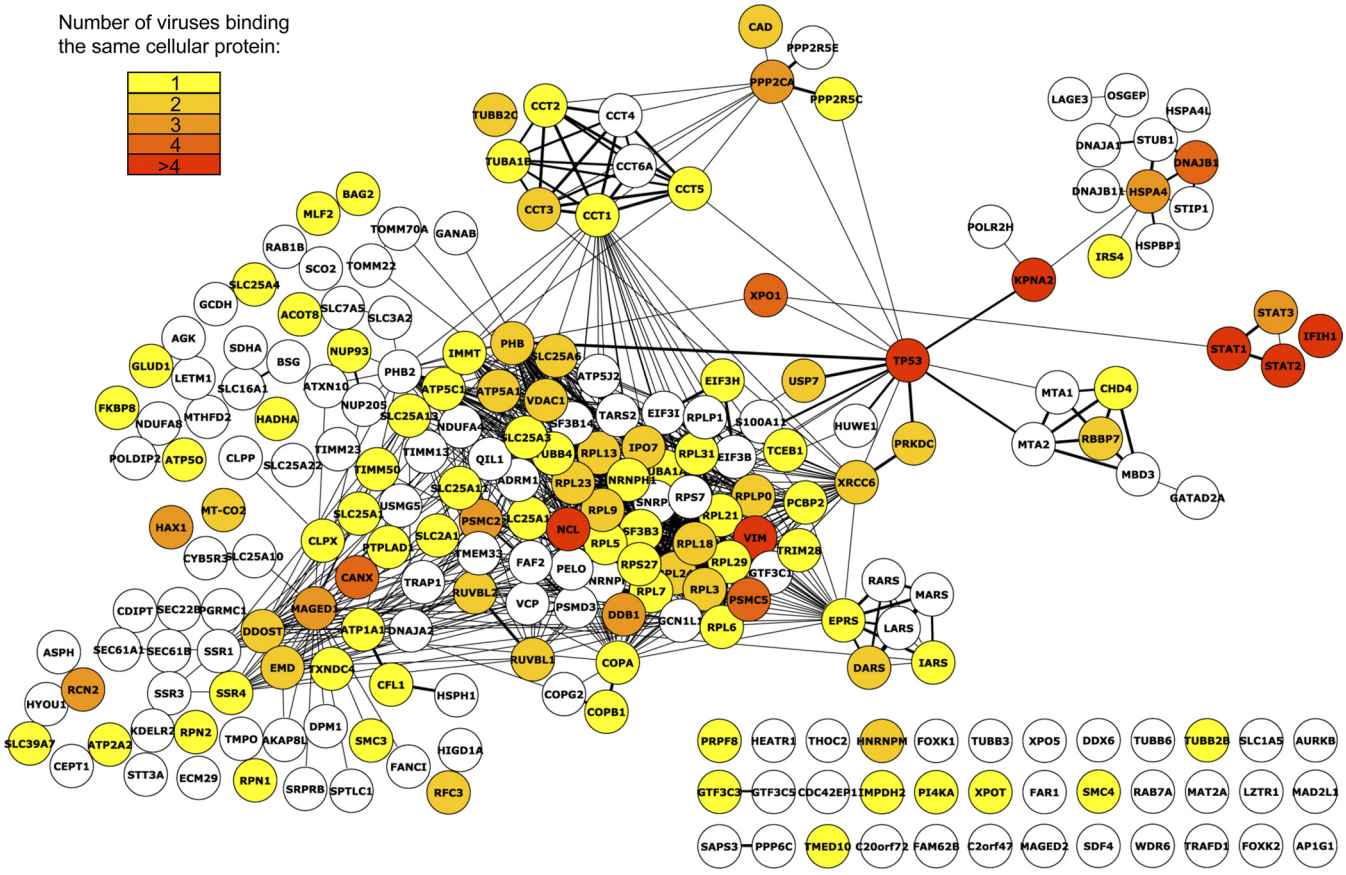


FIG. 10. **MV-V interactors are well-known targets of viruses in general.** VirHostNet database was queried to identify cellular proteins from MV-V interaction map that were previously identified as binding partners of other viruses. A yellow-to-red color range was applied to identify host proteins targeted by 1, 2, 3, 4 or more than 4 distinct viruses.

carrier group of membrane transport protein members (SLC), component of the respiratory chain (cytochrome oxidase) and ATP synthetase, membrane enzymes and proteins involved in cell cycle control (prohibitin). Interestingly, mitochondrial proteins like prohibitin, prohibitin 2, and VDAC1 have been shown to interact with nonstructural protein 2 of severe respiratory syndrome coronavirus (SARS-CoV) (44). In addition, major changes in mitochondrial protein expression profiles have been recently observed in cells infected with human respiratory syncytial virus (RSV), another member of *Paramyxoviridae* family (45). Munday *et al.* used a stable isotope labeling with amino acids in cell culture coupled to LC-MS/MS analyses. They showed substantial changes in the abundance and localization of mitochondrial proteins such as the accessory subunit of the mitochondrial membrane respiratory chain NADH dehydrogenase (NDUFB) and components of mitochondrial import complex: TOM20, TOM22, TOM40, and TOM70, VDAC proteins, prohibitin, prohibitin 2 (45). Interestingly, we found NDUFA4, NDUFA8, Tom22, and Tom70 in the list of MV-V interactors. MV-V association with mitochondria components could rely on IFIH-1 binding. MV-V interaction with IFIH1 has been shown to prevent its oligomerization, but we still ignore whether this prevents IFIH1 interaction with MAVS (46). This latter protein is anchored at the membrane of mitochondria, and is used as a scaffold for downstream signaling components of the innate antiviral response (47). Thus, IFIH1 could be an intermediate that bridges MV-V to mitochondrial membranes. MV-V was also found to interact with multiprotein complexes like the histone deacetylase machinery or protein phosphatase 2A. Interestingly, we have experimental evidences showing MV-V direct binding to subunits of protein phosphatase 2A complex (Caignard *et al.*, manuscript in preparation).

To further demonstrate the functional relevance of the interactors found with MV-V, we selected a subset of proteins and decided to focus on HDAC components. Gene repression is commonly associated with regions of deacetylated histones. Maintenance of deacetylated histones and silent chromatin is an active process mediated by HDAC enzymes. Interestingly, it has been shown that HDAC components counteracting the opposite action on cytokine-induced transcription and histone deacetylase activity is required for optimal cellular defense against virus infection (48–50). This activity can be exceeded on transcriptional level by activation IFN-$\beta$ and interferon-stimulated gene promoters or on post-translational level by post-translational modification of tran-

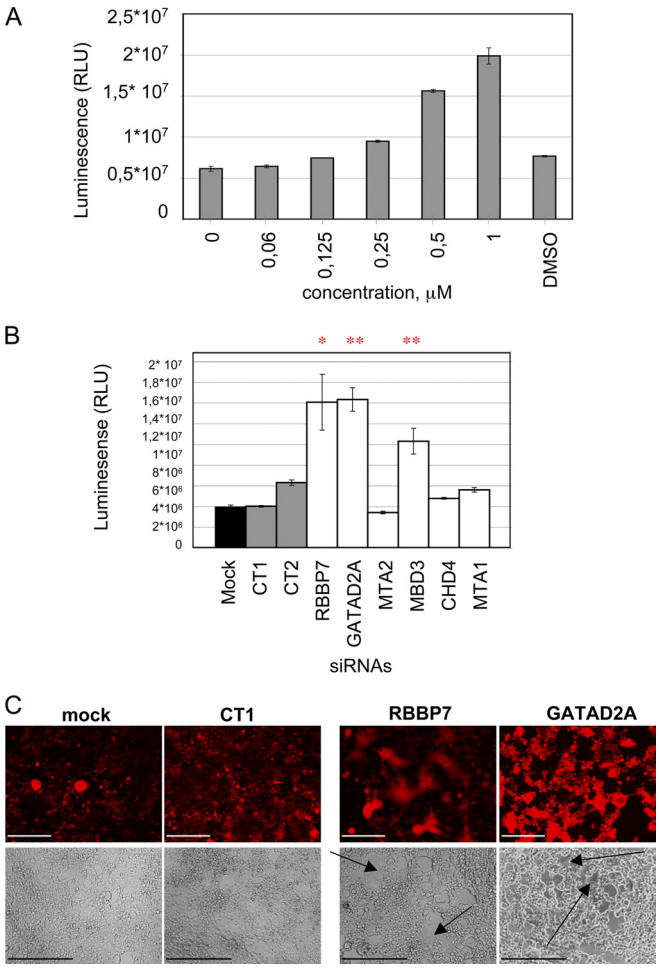


FIG. 11. **Down-regulation of components of histone deacetylase complex (HDAC) up-regulates MV replication.** *A,* Specific HDAC inhibitor TSA up-regulates virus replication. HEK-293T cells were infected with rMV2/Luc at an MOI of 0.2 and treated with TSA at different concentration, mock-treated or mock-treated in the presence of 0.02% DMSO. Luciferase assay was performed 48 h postinfection. Each bar is the means ± S.E. of the mean of luciferase activity measured in duplicate from a representative experiment repeated three times. *B,* and *C,* siRNA-mediated down-regulation of endogenous components of HDAC enhances MV replication in 293T cells. HEK-293T cells were transfected with siRNAs targeting six different components of HDAC complex (RBBP7, GATAD2A, MTA2, MBD3, CHD4, and MTA1), transfected with two control RNAs (CT1 and CT2) or mock-transfected. 24 h post-transfection cells were infected with rMV2//Luc at an MOI of 0.5 and luciferase assay was performed 48 h postinfection. One and two red asterisks demonstrate statistically significant enrichments with $p$ values $<0.05$ and $<0.01$, respectively in Luc production in comparison with mock-transfected cells. Each bar is the mean ± S.E. of the mean of luciferase activity measured in triplicate from a representative experiment repeated three times. *C*, Light and fluorescence microscopy analysis of Cherry protein expression by rMV2/STrEP-CH 48 h postinfection on HEK-293T cells transfected or not with siRNAs against specific components of HDAC complex. Black arrows indicate syncytia formed by infected cells. Fluorescence images were taken with a 5 × objective. Light images were taken with the same objective but magnified 1.5 times with Bertrand lens. White and black scale bars correspond to 500 µm.

scription factors. Consequently, blocking of HDAC activity by specific inhibitors such as TSA has been shown to increase virus cytopathic effect or virus replication for HCV, encephalomyocarditis, vesicular stomatitis, Sendai and Newcastle disease viruses. In the present report, we validated the stimulation of MV replication by TSA (Fig. 11*A* and supplemental Fig. S4). Additionally, this correlated with direct and indirect positive effects on MV replication of another HDAC inhibitor such as valproic acid sodium salt (51). Furthemore, the knockdown of RBBP7, GATAD2A, or MBD3, three HDAC components that specifically interacted with MV-V in a viral context, also increased MV replication (Fig. 11*B*). The fact that HDAC inhibitors and the silencing of the components of histone deacetylase machinery provided analogous effect on MV-replication suggests that in addition to already known MV-V interactions with STAT1, STAT2, JAK1, IFIH1, LGP2, IKK-$\alpha$, IRF7, these new MV-V cellular partners (RBBP7, GATAD2A, MBD3, MTA1, MTA2, and CHD4) may also be important for MV-mediated inhibition of the host innate antiviral response.

Altogether, our data demonstrate the interest of combining virus reverse genetics together with protein complex analysis by nano-LC-MS/MS to decipher virus-host protein interactions. Direct and indirect interactions cannot be distinguished in this approach, but it is extremely valuable because interactions are identified directly from infected cells, in a highly relevant and physiological setting. It also provides a global overview of cellular pathways and functional modules targeted by a viral protein, instead of a limited list of direct interactors that sometimes resist interpretation. This nicely complements other strategies, including yeast two-hybrid technology or protein arrays, which allow the identification of direct protein interactions but are performed in an artificial context that calls for additional validation steps. In the future, the same strategy could be applied to any other negative-strand RNA viruses because a RNA virus could easily develop direct interactions with 60–80 different host proteins according to recent estimations, and only a few percents have been characterized (38). Whatever we do, mapping these interactions is a prerequisite to reach a system level understanding of viral infection process.

*Acknowledgments*—We thank Dr. Kaoru Takeuchi and Dr. Chantal Rabourdin-Combe for anti-V rAb polyclonal antibody and anti-N mAb monoclonal antibody. We thank Thibaut Jacob for updating GO annotation in GOlorize plug-in. We thank all members of the Unité de Génomique Virale et Vaccination for their support.

* This work was supported by the Institut Pasteur and CNRS. Dr. AVK is supported by a "Bourse Roux" (Institut Pasteur).

S This article contains supplemental Figs. S1 to S5 and Tables S1 to S8.

‡‡ To whom correspondence should be addressed: Unité de Génomique Virale et Vaccination, Institut Pasteur, CNRS URA 3015, Paris, France. Tel.: +33 (1) 45 68 87 70; Fax: +33 (1) 40 61 31 67; E-mail: ftangy@pasteur.fr or vidalain@pasteur.fr.

REFERENCES


1. Vidalain, P. O., and Tangy, F. (2010) Virus-host protein interactions in RNA viruses. *Microbes and Infection / Institut Pasteur* **12,** 1134–1143
2. de Chassey, B., Navratil, V., Tafforeau, L., Hiet, M. S., Aublin-Gex, A., Agaugué, S., Meiffren, G., Pradezynski, F., Faria, B. F., Chantier, T., Le Breton, M., Pellet, J., Davoust, N., Mangeot, P. E., Chaboud, A., Penin, F., Jacob, Y., Vidalain, P. O., Vidal, M., André, P., Rabourdin-Combe, C., and Lotteau, V. (2008) Hepatitis C virus infection protein network. *Mol. Syst. Biol.* **4,** 230
3. Shapira, S. D., Gat-Viks, I., Shum, B. O., Dricot, A., de Grace, M. M., Wu, L., Gupta, P. B., Hao, T., Silver, S. J., Root, D. E., Hill, D. E., Regev, A., and Hacohen, N. (2009) A physical and regulatory map of host-influenza interactions reveals pathways in H1N1 infection. *Cell* **139,** 1255–1267
4. Mayer, D., Molawi, K., Martínez-Sobrido, L., Ghanem, A., Thomas, S., Baginsky, S., Grossmann, J., Garcia-Sastre, A., and Schwemmle, M. (2007) Identification of cellular interaction partners of the influenza virus ribonucleoprotein complex and polymerase complex using proteomic-based approaches. *J. Proteome Res.* **6,** 672–682
5. Brizard, J. P., Carapito, C., Delalande, F., Van Dorsselaer, A., and Brugidou, C. (2006) Proteome analysis of plant-virus interactome: comprehensive data for virus multiplication inside their hosts. *Mol. Cell. Proteomics* **5,** 2279–2297
6. Spurgers, K. B., Alefantis, T., Peyser, B. D., Ruthel, G. T., Bergeron, A. A., Costantino, J. A., Enterlein, S., Kota, K. P., Boltz, R. C., Aman, M. J., Delvecchio, V. G., and Bavari, S. (2010) Identification of essential filovirion-associated host factors by serial proteomic analysis and RNAi screen. *Mol. Cell. Proteomics* **9,** 2690–2703
7. Radhakrishnan, A., Yeo, D., Brown, G., Myaing, M. Z., Iyer, L. R., Fleck, R., Tan, B. H., Aitken, J., Sanmun, D., Tang, K., Yarwood, A., Brink, J., and Sugrue, R. J. (2010) Protein analysis of purified respiratory syncytial virus particles reveals an important role for heat shock protein 90 in virus particle assembly. *Mol. Cell. Proteomics* **9,** 1829–1848
8. Billeter, M. A., Naim, H. Y., and Udem, S. A. (2009) Reverse genetics of measles virus and resulting multivalent recombinant vaccines: applications of recombinant measles viruses. *Current Topics Microbiol. Immunol.* **329,** 129–162
9. Conzelmann, K. K. (2004) Reverse genetics of mononegavirales. *Current Topics Microbiol. Immunol.* **283,** 1–41
10. Neumann, G., and Kawaoka, Y. (2004) Reverse genetics systems for the generation of segmented negative-sense RNA viruses entirely from cloned cDNA. *Current Topics Microbiol. Immunol.* **283,** 43–60
11. Cattaneo, R., Kaelin, K., Baczko, K., and Billeter, M. A. (1989) Measles virus editing provides an additional cysteine-rich protein. *Cell* **56,** 759–764
12. Devaux, P., Hodge, G., McChesney, M. B., and Cattaneo, R. (2008) Attenuation of V- or C-defective measles viruses: infection control by the inflammatory and interferon responses of rhesus monkeys. *J. Virol.* **82,** 5359–5367
13. Patterson, J. B., Thomas, D., Lewicki, H., Billeter, M. A., and Oldstone, M. B. (2000) V and C proteins of measles virus function as virulence factors in vivo. *Virology* **267,** 80–89
14. Parisien, J. P., Bamming, D., Komuro, A., Ramachandran, A., Rodriguez, J. J., Barber, G., Wojahn, R. D., and Horvath, C. M. (2009) A shared interface mediates paramyxovirus interference with antiviral RNA helicases MDA5 and LGP2. *J. Virol.* **83,** 7252–7260
15. Caignard, G., Guerbois, M., Labernardière, J. L., Jacob, Y., Jones, L. M., Wild, F., Tangy, F., and Vidalain, P. O. (2007) Measles virus V protein blocks Jak1-mediated phosphorylation of STAT1 to escape IFN-alpha/beta signaling. *Virology* **368,** 351–362
16. Pfaller, C. K., and Conzelmann, K. K. (2008) Measles virus V protein is a decoy substrate for IkappaB kinase alpha and prevents Toll-like receptor 7/9-mediated interferon induction. *J. Virol.* **82,** 12365–12373
17. Caignard, G., Bouraï, M., Jacob, Y., Tangy, F., and Vidalain, P. O. (2009) Inhibition of IFN-alpha/beta signaling by two discrete peptides within measles virus V protein that specifically bind STAT1 and STAT2. *Virology* **383,** 112–120
18. Ramachandran, A., Parisien, J. P., and Horvath, C. M. (2008) STAT2 is a primary target for measles virus V protein-mediated alpha/beta interferon signaling inhibition. *J. Virol.* **82,** 8330–8338
19. Cruz, C. D., Palosaari, H., Parisien, J. P., Devaux, P., Cattaneo, R., Ouchi, T., and Horvath, C. M. (2006) Measles virus V protein inhibits p53 family member p73. *J. Virol.* **80,** 5644–5650
20. Combredet, C., Labrousse, V., Mollet, L., Lorin, C., Delebecque, F., Hurtrel, B., McClure, H., Feinberg, M. B., Brahic, M., and Tangy, F. (2003) A molecularly cloned Schwarz strain of measles virus vaccine induces strong immune responses in macaques and transgenic mice. *J. Virol.* **77,** 11546–11554
21. Guerbois, M., Moris, A., Combredet, C., Najburg, V., Ruffié, C., Février, M., Cayet, N., Brandler, S., Schwartz, O., and Tangy, F. (2009) Live attenuated measles vaccine expressing HIV-1 Gag virus like particles covered with gp160DeltaV1V2 is strongly immunogenic. *Virology* **388,** 191–203
22. Calain, P., and Roux, L. (1993) The rule of six, a basic feature for efficient replication of Sendai virus defective interfering RNA. *J. Virol.* **67,** 4822–4830
23. Giraudon, P., and Wild, T. F. (1981) Monoclonal antibodies against measles virus. *J. Gen. Virol.* **54,** 325–332
24. Takeuchi, K., Kadota, S. I., Takeda, M., Miyajima, N., and Nagata, K. (2003) Measles virus V protein blocks interferon (IFN)-alpha/beta but not IFN-gamma signaling by inhibiting STAT1 and STAT2 phosphorylation. *FEBS Lett.* **545,** 177–182
25. Schaffner, W., and Weissmann, C. (1973) A rapid, sensitive, and specific method for the determination of protein in dilute solution. *Anal. Biochem.* **56,** 502–514
26. Hernandez-Toro, J., Prieto, C., and De las Rivas, J. (2007) APID2NET: unified interactome graphic analyzer. *Bioinformatics* **23,** 2495–2497
27. Shannon, P., Markiel, A., Ozier, O., Baliga, N. S., Wang, J. T., Ramage, D., Amin, N., Schwikowski, B., and Ideker, T. (2003) Cytoscape: a software environment for integrated models of biomolecular interaction networks. *Genome Res.* **13,** 2498–2504
28. Maere, S., Heymans, K., and Kuiper, M. (2005) BiNGO: a Cytoscape plugin to assess overrepresentation of gene ontology categories in biological networks. *Bioinformatics* **21,** 3448–3449
29. Garcia, O., Saveanu, C., Cline, M., Fromont-Racine, M., Jacquier, A., Schwikowski, B., and Aittokallio, T. (2007) GOlorize: a Cytoscape plug-in for network visualization with Gene Ontology-based layout and coloring. *Bioinformatics* **23,** 394–396
30. Aranda, B., Achuthan, P., Alam-Faruque, Y., Armean, I., Bridge, A., Derow, C., Feuermann, M., Ghanbarian, A. T., Kerrien, S., Khadake, J., Kerssemakers, J., Leroy, C., Menden, M., Michaut, M., Montecchi-Palazzi, L., Neuhauser, S. N., Orchard, S., Perreau, V., Roechert, B., van Eijk, K., and Hermjakob, H. (2010) The IntAct molecular interaction database in 2010. *Nucleic Acids Res.* **38,** D525–531
31. Navratil, V., de Chassey, B., Meyniel, L., Delmotte, S., Gautier, C., André, P., Lotteau, V., and Rabourdin-Combe, C. (2009) VirHostNet: a knowledge base for the management and the analysis of proteome-wide virus-host interaction networks. *Nucleic Acids Res.* **37,** D661–668
32. Parks, C. L., Witko, S. E., Kotash, C., Lin, S. L., Sidhu, M. S., and Udem, S. A. (2006) Role of V protein RNA binding in inhibition of measles virus minigenome replication. *Virology* **348,** 96–106
33. Bankamp, B., Lopareva, E. N., Kremer, J. R., Tian, Y., Clemens, M. S., Patel, R., Fowlkes, A. L., Kessler, J. R., Muller, C. P., Bellini, W. J., and Rota, P. A. (2008) Genetic variability and mRNA editing frequencies of the phosphoprotein genes of wild-type measles viruses. *Virus Res.* **135,** 298–306
34. Chen, M., Cortay, J. C., and Gerlier, D. (2003) Measles virus protein interactions in yeast: new findings and caveats. *Virus Res.* **98,** 123–129
35. Devaux, P., and Cattaneo, R. (2004) Measles virus phosphoprotein gene products: conformational flexibility of the P/V protein amino-terminal domain and C protein infectivity factor function. *J. Virol.* **78,** 11632–11640
36. Haynes, C., Oldfield, C. J., Ji, F., Klitgord, N., Cusick, M. E., Radivojac, P., Uversky, V. N., Vidal, M., and Iakoucheva, L. M. (2006) Intrinsic disorder is a common feature of hub proteins from four eukaryotic interactomes. *PLoS Comput. Biol.* **2,** e100
37. Longhi, S., and Oglesbee, M. (2010) Structural disorder within the measles virus nucleoprotein and phosphoprotein. *Protein Pept. Lett.* **17,** 961–978
38. Vidalain, P. O., and Tangy, F. (2010) Virus-host protein interactions in RNA viruses. *Microbes Infect.* **12,** 1134–1143
39. Calderwood, M. A., Venkatesan, K., Xing, L., Chase, M. R., Vazquez, A., Holthaus, A. M., Ewence, A. E., Li, N., Hirozane-Kishikawa, T., Hill, D. E., Vidal, M., Kieff, E., and Johannsen, E. (2007) Epstein-Barr virus and virus human protein interaction maps. *Proc. Natl. Acad. Sci. U. S. A.* **104,** 7606–7611

40. Palosaari, H., Parisien, J. P., Rodriguez, J. J., Ulane, C. M., and Horvath, C. M. (2003) STAT protein interference and suppression of cytokine signal transduction by measles virus V protein. *J. Virol.* **77,** 7635–7644
41. Childs, K., Stock, N., Ross, C., Andrejeva, J., Hilton, L., Skinner, M., Randall, R., and Goodbourn, S. (2007) mda-5, but not RIG-I, is a common target for paramyxovirus V proteins. *Virology* **359,** 190–200
42. Bailer, S. M., and Haas, J. (2009) Connecting viral with cellular interactomes. *Curr Opin. Microbiol.* **12,** 453–459
43. Colina, R., Costa-Mattioli, M., Dowling, R. J., Jaramillo, M., Tai, L. H., Breitbach, C. J., Martineau, Y., Larsson, O., Rong, L., Svitkin, Y. V., Makrigiannis, A. P., Bell, J. C., and Sonenberg, N. (2008) Translational control of the innate immune response through IRF-7. *Nature* **452,** 323–328
44. Cornillez-Ty, C. T., Liao, L., Yates, J. R., 3rd, Kuhn, P., and Buchmeier, M. J. (2009) Severe acute respiratory syndrome coronavirus nonstructural protein 2 interacts with a host protein complex involved in mitochondrial biogenesis and intracellular signaling. *J. Virol.* **83,** 10314–10318
45. Munday, D. C., Emmott, E., Surtees, R., Lardeau, C. H., Wu, W., Duprex, W. P., Dove, B. K., Barr, J. N., and Hiscox, J. A. (2010) Quantitative proteomic analysis of A549 cells infected with human respiratory syncytial virus. *Mol. Cell. Proteomics* **9,** 2438–2459
46. Childs, K. S., Andrejeva, J., Randall, R. E., and Goodbourn, S. (2009) Mechanism of mda-5 Inhibition by paramyxovirus V proteins. *J. Virol.* **83,** 1465–1473
47. Arnoult, D., Carneiro, L., Tattoli, I., and Girardin, S. E. (2009) The role of mitochondria in cellular defense against microbial infection. *Semin Immunol* **21,** 223–232
48. Génin, P., Morin, P., and Civas, A. (2003) Impairment of interferon-induced IRF-7 gene expression due to inhibition of ISGF3 formation by trichostatin A. *J. Virol.* **77,** 7113–7119
49. Nusinzon, I., and Horvath, C. M. (2006) Positive and negative regulation of the innate antiviral response and beta interferon gene expression by deacetylation. *Mol. Cell. Biol.* **26,** 3106–3113
50. Chang, H. M., Paulson, M., Holko, M., Rice, C. M., Williams, B. R., Marié, I., and Levy, D. E. (2004) Induction of interferon-stimulated gene expression and antiviral responses require protein deacetylase activity. *Proc. Natl. Acad. Sci. U. S. A.* **101,** 9578–9583
51. Eugenio, K. R. (2003) Sodium valproate and measles virus replication. *Eur. J. Pediatr.* **162,** 195